MECHANICAL BEHAVIOUR OF INTERPENETRATING Al-SiC COMPOSITES DERIVED FROM WOOD TEMPLATES

T. E. Wilkes[a], J. Y. Pastor[b], J. Llorca[b,c], K. T. Faber[a]

[a]Department of Materials Science and Engineering,
Robert R. McCormick School of Engineering and Applied Science,
Northwestern University, Evanston, IL 60208-3108, USA.

[b]Departamento de Ciencia de Materiales, Universidad Politécnica de Madrid,
[c]Instituto Madrileño de Estudios Avanzados en Materiales (IMDEA-Materiales)
E. T. S. de Ingenieros de Caminos, 28040 Madrid, SPAIN.

ABSTRACT

The mechanical behavior in SiC Al-Si-Mg metal-ceramic composites (50:50 by volume) was studied between 25 and 500 °C. The SiC phase was derived from wood precursors, which resulted in an interconnected anisotropic ceramic that constrained the pressure melt-infiltrated aluminum alloy. The composites were made using SiC derived from two woods (sapele and beech) and were studied in three orthogonal orientations. The mechanical properties and corresponding deformation micromechanisms were different in the longitudinal and transverse directions but the influence of the precursor wood was small. The longitudinal behavior was controlled by the rigid SiC preform and the load transfer from the metal to the ceramic. Moduli in this orientation were less than Halpin-Tsai predictions due to the non-linear and non-parallel nature of the Al-filled pores.

1. INTRODUCTION

The porous silicon carbide (SiC) derived from wood has been widely studied and has been considered for lightweight structural materials, catalyst supports, heat exchangers, high-temperature molten metal filters and composite reinforcements [1-6].

Prior research has shown the viability of infiltrating molten metal into the pore space of wood-derived SiC, but characterization of the resulting metal-ceramic composites (MCCs) was limited to room-temperature mechanical properties [7-9]. The current work aimed to expand upon these findings by studying the mechanical behaviour, and deformation and failure micromechanisms, of MCCs obtained from various wood precursors as a function of temperature.

Wood is a honeycomb-like anisotropic material with pores aligned both parallel and perpendicular to the long axis of the tree, which is commonly referred to as the axial direction [10, 11]. Both the diameter of the pores and the spatial distribution of the pores can vary between wood species. Hardwoods have a bimodal distribution of axially-oriented pores, and the larger- and smaller-diameter pores are referred to as vessels and fibre cells, respectively. The pores running perpendicular to the axial direction, rays are radially-oriented and originate at the centre of the tree. The third orthogonal direction in wood, the tangential direction, is tangent to growth rings: the concentric circles that are often visible to the naked eye. These rings are a result of changing growth rates that affect the diameter of the vessels. Throughout the processing of wood-derived SiC, the wood microstructure is retained and results in a honeycomb-like SiC material. The porosity, spatial distribution and orientation of the pores affect the properties of the porous SiC [12, 13], but the influence of these factors on the mechanical properties of the MCCs are not known.

SiC obtained from wood offers several advantages over traditional ceramic processing methods [1]. Low processing temperatures use less energy than sintering processes, the multitude of different wood species allows for tailored microstructures, and near-net-shape parts can be produced with little or no machining of the ceramic. These advantages make processing composites using melt-infiltration techniques easier, eliminating the need for binders, sintering, or other complexities involved in making cohesive preforms [14]. By applying sufficiently high temperatures and pressures, dense parts can be produced without concern for metal-ceramic wettability; however,

reactions between the molten metal and ceramic may occur and lead to impurities in the composite. For example, pure aluminium reacts with SiC to form aluminium carbide (Al_4C_3), a brittle intermetallic compound that can diminish mechanical properties [15]. Alloying additions of silicon and magnesium deter this reaction, and improve wetting between Al and SiC. The particular aluminium alloy used in this work, containing 13 wt.% Si and 9 wt.% Mg, was shown to optimize these effects in SiC-Al composites [16]. Addition of a metal to a brittle ceramic can increase the toughness and ductile response of the material while retaining most of the stiffness and strength imparted by the ceramic [17, 18]. By using a porous preform, the metal acts as a system of ductile inclusions within the interconnected ceramic. Increased mechanical behaviour results from mechanisms such as plastic stretching of the inclusions, decohesion between the metal and ceramic, and fracture of the ceramic phase near the inclusions, all of which increase the work required for crack propagation [19, 20]. As well, residual stresses can increase the initial force needed for crack growth and induce plastic strain in inclusions, which can act to shield a crack tip [18].

The objective of this work is to study the mechanical properties and the underlying deformation, and fracture micromechanisms of the wood-derived SiC Al alloy MCCs from 25 to 500 °C. The composite properties are compared to those of the Al-Si-Mg alloy and, where data are available, to the porous wood-derived SiC. Predictions for the elastic modulus are obtained from constituent properties and Halpin-Tsai bounds [21]. Comparisons of the model predictions with the experimental results provide information on the main microstructural factors which control the mechanical behaviour of the novel composites as a function of temperature and orientation.

2. EXPERIMENTAL DETAILS

2.1 Sample processing

Two hardwoods were used as starting materials: beech (*BE*) and sapele (*SA*). The process to manufacture the MCCs involved first pyrolyzing the wood in an Ar atmosphere at 1000 °C for one hour. Next, the resulting amorphous carbon was heated in vacuum to 1550 °C for another hour with a stoichiometric excess of silicon powder (99.6 wt.% Si). Once molten, the silicon reacted with the carbon to form β-SiC. This reaction promoted wetting, and the Si was wicked into the cylindrical pores. If required, this reaction step was repeated to reduce the amount of residual C in the specimens.

After solidification, some pores retain excess silicon, which can be removed by using carbon felt or an acid etch. Using carbon felt requires reheating the Si/SiC material to above the melting point of Si in an inert atmosphere. The felt wicks the excess Si out of the pores, but some residual Si may still remain. An acid solution consisting of 50:50 vol.% concentrated hydrofluoric and nitric acids can also be used to remove the excess silicon. The nitric and hydrofluoric acids act to cyclically oxidize the Si into SiO_2 and etch away the SiO_2, respectively. In this work, samples were etched for at least 14 days to ensure complete removal of the excess silicon. In the final processing step, the porous SiC preforms were melt-infiltrated with an Al-13Si-9Mg alloy using a gas-pressure liquid-metal infiltration furnace [8, 22]. A cast cylinder of the alloy was placed on top of specimens in a graphite crucible. The furnace was heated in vacuum to 750 °C whereupon the aluminium alloy melted and formed a seal with the crucible walls, isolating the porous SiC in a vacuum environment. The furnace was then pressurized, using high-purity argon, to 3.5 MPa, which forced the molten aluminium alloy into the pores. The density of the SiC preforms, Al-Si-Mg alloy, and MCCs were measured using Archimedes' method as detailed in ASTM-C373 [23].

2.2 Mechanical characterization

Following the procedures above, MCC bars measuring 3.0 mm x 3.0 mm x 30 mm were machined to measure the bending strength and elastic modulus. All bend tests were carried out in a three-point bend configuration as shown schematically in Fig. 1, which also depicts the three specimen orientations. The Al-filled pores in longitudinal (*LO*) samples are oriented normal to fracture surfaces. Transverse samples are oriented

with the Al-filled pores lying in the fracture plane and either parallel (*TR1*) or perpendicular (*TR2*) to the applied load. Bars of the Al-Si-Mg alloy were also machined and tested using the same dimensions and specifications as the MCC specimens. Flexural strength tests were conducted with an Instron 8501 mechanical testing machine, and a frame-mounted MTS 653 modified furnace was used to heat specimens for tests above room-temperature. A linear variable differential transducer was used to measure the displacement. Tests were conducted using a displacement rate of 100 μm/min, a heating rate of 10 °C/min and a hold time of 20 minutes. The flexural strength, σ_f, was calculated according to ASTM C1161 [24] using between three and six samples for each testing condition. Specimen microstructures, fracture surfaces, and crack paths were examined by scanning electron microscopy (Hitachi S3400N).

Tests to measure the evolution of the flexural modulus with temperature were carried out in an Instron 4505 mechanical testing machine with a custom-built furnace (Entech, Sweden). The mid-span deflection of the bend bar was measured through a quartz window in the furnace using a high-resolution laser extensometer (Zygo 2211). The displacement rate, heating rate, and hold time were 100 μm/min, 10 °C/min, and 20 minutes, respectively. The flexural modulus was calculated from the slope of force versus mid-span displacement curves [24]. For each material and orientation, one specimen was used to measure elastic loading-unloading curves for the entire range of testing temperatures. After each measurement, the specimen was heated to the next set-point and held for 20 minutes before repeating the loading-unloading measurement.

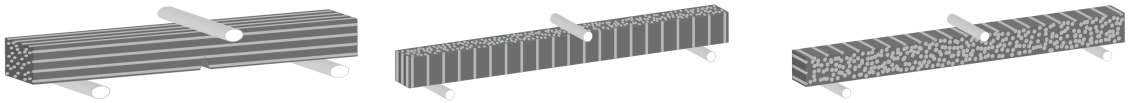

Figure 1. Bend test sample orientations: longitudinal (LO) specimen (left) and transverse 1 (TR1) and 2 (TR2) specimens, middle and right respectively.

Tensile testing of the aluminium alloy was conducted in an MTS 808 mechanical testing machine, a frame-mounted ATS 3210 furnace, and an extensometer (MTS 632-13B-21). Tests were carried out under displacement control with a displacement rate of 1 mm/min. Samples tested above room-temperature were heated under load-control without a programmed heating rate. Before testing, the temperature was held until the extensometer reading stabilized, i.e. when both the specimen and fixture had reached thermal equilibrium. The Young's modulus of the aluminium alloy was measured as the slope of the tensile stress versus strain curve, and the yield strength was calculated using the offset method at 0.2% strain.

3. RESULTS

3.1. Microstructure

Micrographs of both axial and radial sections of BE- and SA-derived C, SiC, and MCCs are shown in Fig. 2(a)-(d), (e)-(h), and (i)-(l), respectively. The replicated wood characteristics, including the three cell types, are most evident in the carbon cross-sections. The axially-oriented pores propagate into and out of the page in the axial sections and vertically in the radial sections. The radially-oriented pores are vertical in the axial sections and run into and out of the page in the radial sections. In Fig. 2a, the radial pores, indicated by the vertical arrow, intersect a relatively dense horizontal band, indicated by the horizontal arrow that separates the late wood (bottom) from early wood (top). The features of SA specimens are generally larger than the BE counterparts, but the late to early wood transitions are less distinct, i.e. pore diameters remain relatively constant throughout growth seasons.

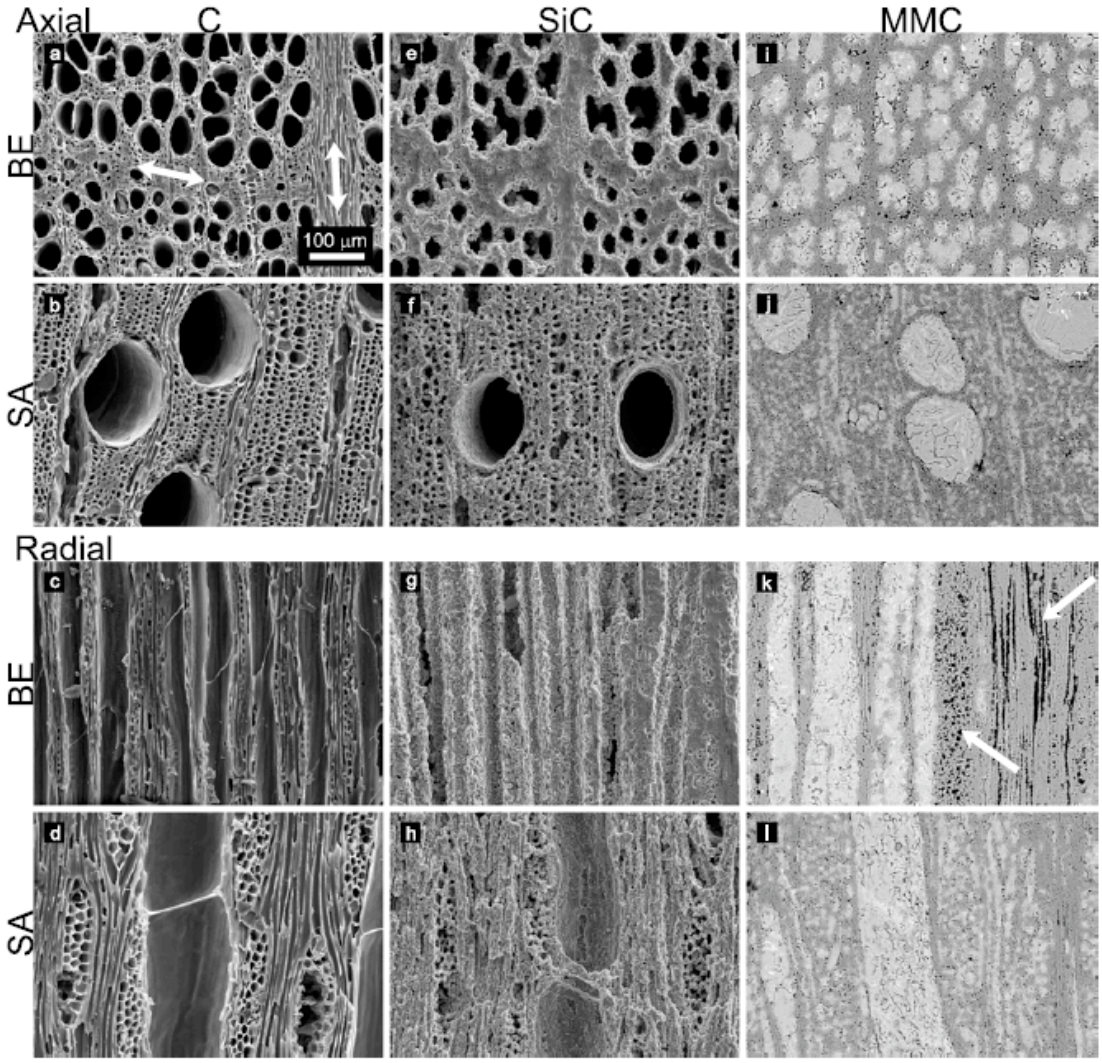

Figure 2. SEM micrographs of the BE- and SA-C and -SiC, and back-scattered electron micrographs of the BE- and SA-MCCs. Cross-sections are perpendicular to either the axial direction (top) or radial direction (bottom). BE and SA micrographs are on the top and bottom of each half, respectively, and the columns depict, from left to right, the C, SiC, and MCCs. In (a), the vertical arrow indicates the band of radially-oriented pores and the late- and early wood are separated by the horizontal arrow. In (j), the arrow points to an area of decohesion along the metal-ceramic interface. In (k), the arrows point to closed porosity oriented in both the radial (left) and axial (right) directions.

Upon conversion to SiC, the reaction between molten silicon and amorphous carbon to form SiC was accompanied by a volume change of about 50% [25]. While the overall specimen dimensions did not significantly change, the volume change was accommodated within the pores. This resulted in decreased pore diameters, but some of the pore walls in the BE specimens were damaged, which led to some effectively larger pores (Fig. 2e). Most of the smaller diameter pores were no longer present in the BE-SiC (Fig. 2e and 2g) but were observed in the SA-SiC (Fig. 2f and 2h).

A one-hour hold at 1550 °C was insufficient to completely convert the entire C scaffold to SiC for the sample sizes used in this study. As carbon in a smaller pore reacted and the pore closed due to the volume expansion, a barrier was formed, which impeded further reaction to form the SiC. Most of the residual C was converted to SiC after repeating this reaction step. Small amounts of residual carbon were observed in both specimen types. Based on the theoretical SiC density of 3.21 g/cm^3, specific gravity measurements of the BE- and SA-SiC, shown in Table 1, indicated the presence of 4 vol.% residual carbon. This is an upper bound as the calculation did not take into

account any closed porosity in the specimens, which can result from the volume expansion and is visible in the BE-MCC shown in Fig. 2k. The areas indicated by the arrows correspond to small-diameter pores that were pinched closed due to the volume expansion that occurs during the C → SiC reaction.

Table 1. Apparent porosity and specific gravity of beech- and sapele-SiC and MCCs.

	Apparent porosity (%)	Apparent specific gravity (g/cm^3)
BE-SiC	50 ± 3	3.14 ± 0.02
SA-SiC	51 ± 3	3.18 ± 0.03
BE-MCC	4 ± 2	2.84 ± 0.02
SA-MCC	5 ± 3	2.82 ± 0.07
Al-Si-Mg	5 ± 3	2.49 ± 0.04

All four MCC images (Fig. 2i-l) were captured in back-scattered electron mode, and the infiltrated aluminium appeared lighter than the SiC. The porosity and specific gravity of both the MCC and bulk metal, which contained shrinkage porosity, are reported in Table 1. The microstructure was made up of a continuous Al phase (light gray) that included both elongated crystals of primary Si (dark gray) and irregularly-shaped Mg_2Si precipitates (black), which were identified using energy dispersive X-ray spectroscopy. The overall microstructure was similar in both materials and was typical of hypereutectic Al-Si-Mg alloys that were slowly cooled from processing temperatures [26]. The Si crystals in the bulk alloy were larger than those in the composites because the pore size limited growth in the latter. Also, SiC is known to catalyze the nucleation of Si crystals in composites with hypereutectic Al-Si alloys. This results in grain refinement and a larger number of primary Si crystals per unit volume [27].

3.2. Flexural test data

3.2.1. Flexural modulus

The flexural modulus of the MCCs and Al alloy are shown as a function of temperature for each orientation in Fig. 3. The dashed lines represent Halpin-Tsai predictions [21], which were calculated according to:

$$\frac{E^*}{E_{Al}} = \frac{1+\xi\eta V_{SiC}}{1-\eta V_{SiC}} \qquad (1) \qquad \text{and} \qquad \eta = \frac{E_{SiC}/E_{Al} - 1}{E_{SiC}/E_{Al} + \xi} \qquad (2)$$

where E^* is the composite modulus and E_{Al} is the modulus of the aluminium alloy, which was taken as the experimentally-measured flexural modulus of the bulk metal. The modulus of the SiC, E_{SiC}, was assumed to be almost constant in the temperature range of this study, and was taken to be 408 GPa, which has been previously measured by nanoindentation of the wood-derived SiC [28]. For simplicity, the SiC volume fraction, V_{SiC}, was taken as 0.50 for both the BE- and SA-MCCs. For a fiber-reinforced metal matrix composite, the empirical factor, ξ, is a function of both the reinforcement geometry and distribution and also of the composite loading conditions. For this work, the ξ values used were those reported for uniaxial composites: infinity for the LO orientation and 0.50 for the TR1 and TR2 orientations [21]. It should be noted that, in the case of $\xi \to \infty$, Equation 1 reduces to the Voigt isostrain model, and in the case $\xi \to 0$, Equation 1 reduces to the Reuss isostress model.

The modulus of the bulk aluminium alloy remained relatively constant at about 70 GPa from 25 to 300 °C, decreased between 300 and 400 °C to 30 GPa, and was too compliant to reliably test at 500 °C. The elastic moduli of the LO-MCCs remained relatively constant at about 200 GPa up to 300 °C and decreased linearly above this temperature to about 130 GPa at 500 °C. The Halpin-Tsai predictions overestimated the stiffness of the BE- and SA-MCCs in the LO orientation. The moduli in the transverse orientations were lower than those of the LO specimens and decreased linearly from a maximum stiffness of about 130 GPa at 25 °C to a minimum of about 85 GPa at 500

°C. Agreement between the Halpin-Tsai calculations and the transverse data was, in general, better than that in the LO orientation:

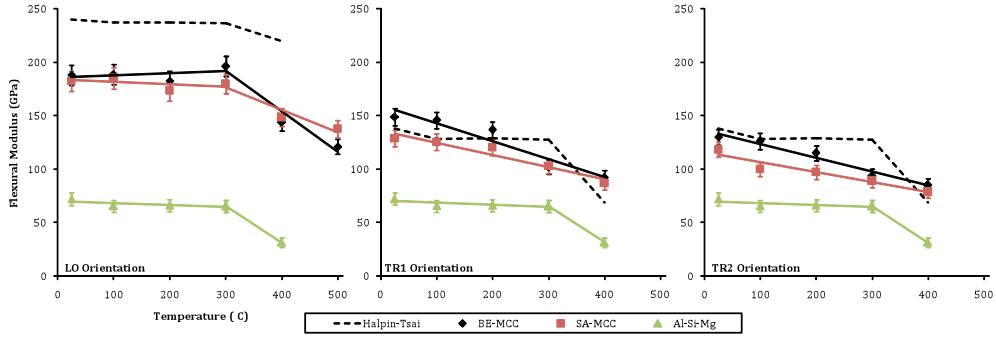

Figure 3. Flexural modulus versus temperature for the LO, TR1, and TR2 orientations of the BE- and SA-MCCs and the bulk Al-Si-Mg alloy from Reference 29. The dashed lines represent Halpin-Tsai predictions for the modulus of a uniaxial composite [21]. The error bars represent one standard deviation.

3.2.2. Flexural strength

The composites presented linear-elastic behaviour until fracture in the longitudinal direction regardless of test temperature and despite evidence of extensive plastic deformation of the metal at high-temperature. The room-temperature load-displacement curves in the transverse directions were also linear-elastic until fracture in all cases, but the BE-MCCs tested in the TR2 orientation showed serrations in the curves. The serrations are indicative of intermittent crack propagation due to differences in the microstructure along the crack path. The specimens tested in the transverse orientations at high-temperature showed non-linear load-displacement curves and the degree of non-linearity increased with temperature.

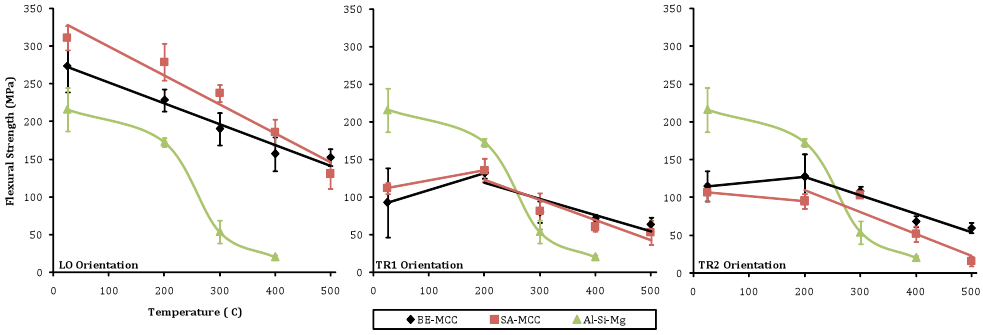

Figure 4. Flexural strength versus temperature for the LO, TR1, and TR2 orientations of the BE- and SA-MCCs and the bulk Al-Si-Mg alloy from Reference 29. The error bars represent one standard deviation.

The average value of the flexural strength of the MCCs and of the Al alloy are shown as a function of temperature for each orientation in Fig. 4. The strength of the bulk Al-Si-Mg decreased slightly between 25 and 200°C, from 215 MPa to 170 MPa, and was drastically weaker at higher temperatures. As was the case with the elastic modulus, the strength of the MCCs was anisotropic, and the specimens tested in the longitudinal direction were consistently stronger than those tested in the TR1 and TR2 orientations over the entire temperature range. Moreover, the evolution of the flexural strength with temperature was different in the longitudinal and transverse orientations.

The longitudinal strength decreased linearly from about 300 MPa at 25 °C to 150 MPa at 500 °C and was always greater than that of the metal. In contrast, the transverse strengths were constant within the experimental scatter from ambient temperature up to

200 °C and these composites were weaker than the bulk Al-Si-Mg alloy. The transverse strengths decreased linearly from 200 to 500 °C but the composites were stronger than the bulk alloy above 200 °C.

4. DISCUSSION

4.1. Elastic behaviour

The room-temperature elastic moduli of BE-MCCs have been previously measured, using pulse-echo ultrasonic velocity measurements, and were reported as 158 GPa and 91-119 GPa for LO and TR samples, respectively [8]. The results for the modulus in bending (Fig. 3) were higher at ambient temperature, but these composites contained less residual porosity and carbon when compared to the samples tested using pulse-echo. The elastic moduli of the MCCs in the longitudinal direction also compared well to results published for SiC particle (SiC_p)-reinforced Al-Si-Mg MCCs prepared by pressureless infiltration. Moduli from 165 GPa to 226 GPa were reported for samples with 41-54 vol.% SiC and 3-8 vol.% porosity [30]. In order to gauge the Al alloy contribution to the composite stiffness, a comparison with the porous wood-derived SiC is needed. The elastic moduli of BE- and SA-SiC, measured in compression with the applied load in the axial direction, were 116 GPa and 23 GPa, respectively, while the moduli with the load perpendicular to the pore channels was 16 GPa and 7 GPa [12]. These data indicated that the microstructure, i.e. spatial distribution of pores for a given volume fraction of porosity, strongly influenced the SiC mechanical properties, but this was not the case for the MCCs.

The moduli for the BE- and SA-MCCs were equal within experimental error, which suggests that eliminating the porosity via aluminium infiltration decreases the influence of the wood characteristics. This leads to a stronger dependence on the volume fractions of the ceramic and metal phases and on the test orientation. The SA-SiC benefits more from the Al-infiltration, where LO and TR moduli were improved by factors of 11 and 18, respectively, as compared to improvements of less than two- and six-fold for the BE-SiC. The larger increases in TR moduli (18 and 6 times greater) versus the LO moduli (11 and <2 times greater) correspond to a reduction in the anisotropy in the moduli of the composites.

The stiffness of porous materials, such as wood-derived SiC, is dependent on microstructural features including the connectivity and thickness of the pore walls, presence of defects, and orientation [31]. Variations in these features can change the dominant deformation mode from stretching to bending and will alter the stiffness of the material. In contrast, the stiffness of the MCCs is controlled by load transfer between phases, which depends on the spatial distribution of phases [21]. In the case of the BE- and SA-MCCs, the microstructure consists of a three-dimensionally continuous SiC phase and long Al alloy fibres oriented in the longitudinal direction. The elastic behavior of this microstructure should follow an isostrain model in the longitudinal direction and an isostress model in the transverse orientations. While agreement between the Halpin-Tsai model and the transverse data is relatively good, the LO data fall well below the predicted stiffnesses. This is due to pore morphology of the wood-derived SiC and the structure of the resulting MCCs [28]. While the Halpin-Tsai calculations are based on an ideal structure, the MCCs contain a non-ideal microstructure with non-linear and non-parallel Al-filled pores. In addition to the decreased stiffness associated with the non-ideal wood precursor microstructure, another possible source of experimental scatter is interface decohesion. Instances of decohesion, which were observed in both the BE- and SA-MCCs, were more apparent in the SA-MCCs. Interface decohesion can be triggered by the residual stresses which develop upon cooling after melt-infiltration due to the thermal expansion mismatch between the SiC and the Al alloy.

4.2. Bending strength and fracture mechanisms

At room temperature, the load-displacement curves corresponding to the bending and fracture tests of the Al alloy were linear elastic until fracture. This brittle behaviour is a result of the presence of the large primary Si crystals. Actually, the strain-to-failure in tension of the Al-Si-Mg alloy at 25 °C was only 0.7% and the ductility increased with temperature up to 8.5% at 400 °C. Composite specimens tested in the longitudinal orientation also presented linear elastic behaviour at ambient temperature, and the non-linearity in the load-displacement curves was limited even at 500 °C. This behaviour reflects the presence of a continuous SiC phase which limits macroscopic plastic deformation; while the Al fibres in the fracture surfaces showed little evidence of plastic deformation at 25 °C (Fig. 5a), the infiltrated Al tended to span the crack opening and then fail by ductile mechanisms of void nucleation and growth at high temperatures. Fig. 5b presents a lateral view in which a bridging metal inclusion has completely failed during a test at 500 °C. The data from the current study agree with data for SiC_p-reinforced Al-Si-Mg MCCs with 41-54 vol.% SiC and 3-8 vol.% residual porosity, which were between 183 MPa and 298 MPa [30].

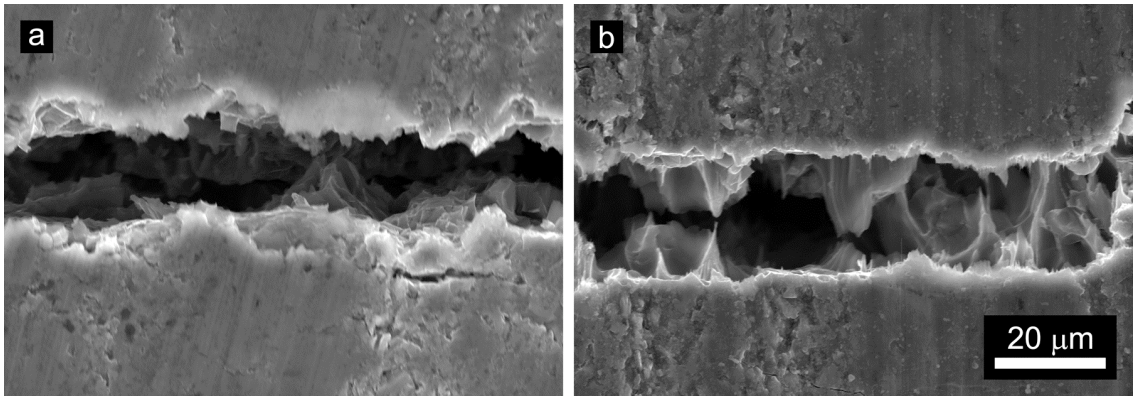

Figure 5. SEM micrographs of fractured BE-MCC specimens in the LO orientation: (a) 25°C crack profile showing brittle fracture and (b) 500°C crack profile showing ductile pullout of the metal at high-temperature.

The MMCs specimens tested in the transverse orientations presented brittle behaviour at ambient temperature, which corresponds with the straight crack paths observed and with the brittle appearance of the fracture surfaces, as shown in Fig. 6a of a BE-MCC tested in the TR2 orientation. Extensive contribution of the plastic deformation of the Al alloy to the non-linear behaviour in the load-displacement curves was observed at high-temperature (Figs. 6b). The bending strength in the TR1 and TR2 orientations of the beech-based composites at 25°C were equivalent to those measured in specimens infiltrated with pure aluminium, which had strengths of 81 MPa and 92-95 MPa for the TR1 and TR2 orientation, respectively [7]. The load-displacement curves of the pure Al-MCCs also exhibited serrations, which was attributed to the varying density resulting from the growth rings. This is supported by results from the current work: the serrations were observed in the BE-TR2 MCCs but not in the SA-TR2 specimens, which lacked the repetitive density changes due to growth rings.

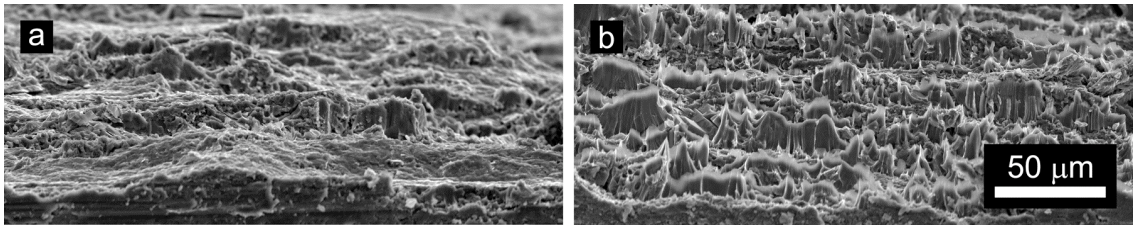

Figure 6. SEM micrographs of BE-MCC in the TR2 orientation: (a) 25°C fracture surface showing the brittle fracture due to the large Si crystals and Mg_2Si precipitates, (b) 500°C fracture surface showing the ductile behaviour of the metal at high-temperature.

5. CONCLUSIONS

Melt-infiltration of an aluminium alloy into porous wood-derived SiC is an effective means to manufacture metal-ceramic composites. The resulting material consists of interconnected SiC with Al fibres oriented in the axial and radial directions of the precursor wood. The modulus and strength in the longitudinal direction were similar to those reported in metal-ceramic composites with equivalent volume fractions of both phases. The corresponding properties in the transverse direction were lower and this behaviour reproduced the differences observed in the properties of the porous SiC. In general, the room temperature strength was maintained up to 200 °C and then decreased due to the marked reduction of the flow stress of the Al alloy above this temperature. The microstructure of the precursor wood had little influence on the stiffness and strength of the MCCs, as opposed to the behaviour found in the porous SiC. The analysis of the experimental results showed that the deformation of the composites in the longitudinal direction was controlled by the rigid SiC skeleton, leading to brittle behaviour all over the entire temperature range. Though load transfer from the Al to the SiC was efficient, the longitudinal composite stiffness was below that predicted by Halpin-Tsai due to the non-ideal microstructure. In the transverse orientation, the Al alloy played a more important role, as it was showed. The stiffness of the TR1 and TR2 MCCs were closer to the Halpin-Tsai model for the transverse stiffness of a uniaxial composite indicating that the load transfer from the Al to the SiC in the transverse direction was less efficient, leading to a lower modulus and strength.

ACKNOWLEDGEMENTS

The work presented in this paper has been funded by grants DMR-0244258/0710630 from the U.S. National Science Foundation, MAT2006-13005-C03-C02 and MAT2007-29278-E from the Ministerio de Educación y Ciencia and S-0505/MAT-0077, and from the Comunidad de Madrid

REFERENCES

1- J. Martinez-Fernandez, F.M. Valera-Feria, M. Singh, “High temperature compressive mechanical behaviour of biomorphic silicon carbide ceramics”, *Scripta Materialia*. 43 (2000) 813-818.

2- J. Martinez-Fernandez, F.M. Valera-Feria, M. Singh, “High temperature compressive mechanical behaviour of biomorphic silicon carbide ceramics”, *Scripta Materialia*. 43 (2000) 813-818.

3- M. Presas, J.Y. Pastor, J. Llorca, A.R. de Arellano-Lopez, J. Martinez-Fernandez, R.E. Sepulveda, “Mechanical behavior of biomorphic Si/SiC porous composites”, *Scripta Materialia*. 53 (2005) 1175-1180.

4- M. Singh, J.A. Salem, “Mechanical properties and microstructure of biomorphic silicon carbide ceramics fabricated from wood precursors”, *J. Eur. Ceram. Soc*. 22 (2002) 2709-2717.

5- M. Singh, B.M. Yee, “Reactive processing of environmentally conscious, biomorphic ceramics from natural wood precursors”, *J. Eur. Ceram. Soc*. 24 (2004) 209-217.

6- F.M. Varela-Feria, J. Martinez-Fernandez, A.R. de Arellano-Lopez, M. Singh, “Low density biomorphic silicon carbide: microstructure and mechanical properties”, *J. Eur. Ceram. Soc*. 22 (2002) 2719-2725.

7- A. Herzog, U.F. Vogt, S. Siegmann, O. Beffort, “Aluminium metal matrix composites based on biomorphic SiC”, *Adv. Eng. Mat*. 8 (2006) 980-983.

8- T.E. Wilkes, M.L. Young, R.E. Sepulveda, D.C. Dunand, K.T. Faber, “Composites by aluminium infiltration of porous silicon carbide derived from wood precursors”, *Scripta Materialia*. 55 (2006) 1083-1086.

9- C. Zollfrank, N. Travitzky, H. Sieber, T. Selchert, P. Greil, “Biomorphous SiSiC/Al-Si ceramic composites manufactured by squeeze casting: Microstructure and mechanical properties”, *Adv. Eng. Mat*. 7 (2005) 743-746.

10- J.M. Dinwoodie, “Wood: nature's cellular, polymeric”, *Fibre-Composite, Institute of Metals*, London; Brookfield, VT, USA, 1989.
11- L.J. Gibson, M.F. Ashby, *Cellular solids: Structure and Properties*, 2nd, Cambridge University Press, Cambridge; New York, 1997.
12- V.S. Kaul, K.T. Faber, R. Sepulveda, A.R. de Arellano-López, J. Martinez-Fernandez, “Precursor Selection and its Role in the Mechanical Properties of Porous SiC Derived from Wood”, *Mat. Scien. and Eng. A*. (2006) In Press.
13- K.E. Pappacena, K.T. Faber, H. Wang, W.D. Porter, “Thermal conductivity of porous silicon carbide derived from wood precursors”, *J. Am. Ceram. Soc*. 90 (2007) 2855-2862.
14- A. Mortensen, V.J. Michaud, M.C. Flemings, “Pressure-infiltration processing of reinforced aluminium”, *JOM-J. Min. Met. & Mat. Soc.* 45 (1993) 36-43.
15- A.C. Ferro, B. Derby, “Wetting Behaviour in the Al-Si/SiC system - interface reactions and solubility effects”, *Acta Metall. Mater*. 43 (1995) 3061-3073.
16- M.I. Pech-Canul, R.N. Katz, M.M. Makhlouf, “Optimum parameters for wetting silicon carbide by aluminum alloys”, *Metal. & Ma. Trans. A* 31 (2000) 565-573.
17- B.D. Flinn, C.S. Lo, F.W. Zok, A.G. Evans, “Fracture-resistance characteristics of a metal-toughened ceramic”, *J. Am. Ceram. Soc.* 76 (1993) 369-375.
18- L.S. Sigl, P.A. Mataga, B.J. Dalgleish, R.M. McMeeking, A.G. Evans, “On the toughness of brittle materials reinforced with a ductile phase”, *Acta Metallurgica*. 36 (1988) 945-953.
19- M.F. Ashby, F.J. Blunt, M. Bannister, “Flow characteristics of highly constrained metal wires”, *Acta Metallurgica*. 37 (1989) 1847-1857.
20- H.E. Dève, S. Schmauder, “Role of interface properties on the toughness of brittle matrix composites reinforced with ductile fibers”, *J. Mater. Res*. 7 (1992) 3132-3138.
21- K.K. Chawla, *Composite Materials: Science and Engineering*, 2nd, Springer, New York, 1998.
22- J.T. Blucher, “Discussion of a Liquid-metal pressure infiltration process to produce metal matrix composites”, *J. of Mat. Processing Technology*. 30 (1992) 381-390.
23- ASTM, ASTM C373-88: *Standard Test Method for Water Absorption, Bulk Density, Apparent Porosity, and Apparent Specific Gravity of Fired Whiteware Products*. 1988, ASTM International: West Conshohocken, PA.
24- ASTM, ASTM C1161-02c: *Standard Test Method for Flexural Strength of Advanced Ceramics at Ambient Temperature*. 2003, ASTM International: West Conshohocken, PA.
25- Y.X. Wang, S.H. Tan, D.L. Jiang, “The effect of porous carbon preform and the infiltration process on the properties of reaction-formed SiC”, *Carbon*. 42 (2004) 1833-1839.
26- Q.G. Wang, C.J. Davidson, “Solidification and precipitation behaviour of Al-Si-Mg casting alloys”, *J. Mater. Sci*. 36 (2001) 739-750.
27- A. Mortensen, I. Jin, “Solidification processing of metal matrix composites”, *International Materials Reviews*. 37 (1992) 101-128.
28- V.S. Kaul, K.T. Faber, “Nanoindentation analysis of the elastic properties of porous SiC derived from wood”. (2008), doi:10.1016/j.scriptamat.2008.01.018.
29- T. E. Wilkes, J. Y. Pastor, J. Llorca, and K. T. Faber, “Mechanical Properties of Wood-Derived Silicon Carbide Aluminum–Alloy Composites as a Function of Temperature,” to appear in *Journal of Materials Research, June 2008.*
30- M.I. Pech-Canul, M.M. Makhlouf, “Processing of Al-SiCp metal matrix composites by pressureless infiltration of SiC_p performs”, *Journal of Materials Synthesis and Processing*. 8 (2000) 35-53.
31- A.R. Studart, U.T. Gonzenbach, E. Tervoort, L.J. Gauckler, “Processing routes to macroporous ceramics: a review”, *J. Am. Ceram. Soc.* 89 (2006) 1771-1789.